the plant journal

Society for Experimental Biology

The Plant Journal (2018) **93,** 943–958 doi: 10.1111/tpj.13822

Biosynthesis of bioactive diterpenoids in the medicinal plant *Vitex agnus-castus*

Allison M. Heskes[1,2,3,*], Tamil C.M. Sundram[1,4], Berin A. Boughton[5], Niels B. Jensen[6], Nikolaj L. Hansen[1,2,3], Christoph Crocoll[7], Federico Cozzi[1], Simon Rasmussen[8], Britta Hamberger[1,2,3], Björn Hamberger[1,2,3], Dan Staerk[9], Birger L. Møller[1,2,3] and Irini Pateraki[1,2,3]

[1]*Plant Biochemistry Laboratory, Department of Plant and Environmental Sciences, University of Copenhagen, Thorvaldsensvej 40, DK-1871 Frederiksberg C, Denmark,*

[2]*Center for Synthetic Biology 'bioSYNergy', Department of Plant and Environmental Sciences, University of Copenhagen, Thorvaldsensvej 40, DK-1871 Frederiksberg C, Denmark,*

[3]*VILLUM Center for Plant Plasticity, Department of Plant and Environmental Sciences, University of Copenhagen, Thorvaldsensvej 40, DK-1871 Frederiksberg C, Denmark,*

[4]*Department of Plant Science, Kulliyyah of Science, International Islamic University Malaysia, 50728 Kuala Lumpur, Malaysia,*

[5]*Metabolomics Australia, School of BioSciences, The University of Melbourne, Vic. 3010, Australia,*

[6]*Evolva A/S, Lersø Parkallé 42-44, DK-2100 Copenhagen Ø, Denmark,*

[7]*DynaMo Center, Department of Plant and Environmental Sciences, University of Copenhagen, Thorvaldsensvej 40, DK-1871 Frederiksberg C, Denmark,*

[8]*Department of Bio and Health Informatics, Technical University of Denmark, DK-2800 Lyngby, Denmark, and*

[9]*Department of Drug Design and Pharmacology, Faculty of Health and Medical Sciences, University of Copenhagen, DK-2100 Copenhagen, Denmark*

Received 29 June 2017; revised 4 December 2017; accepted 14 December 2017; published online 8 January 2018.
*For correspondence (e-mail amh@plen.ku.dk).

SUMMARY

Vitex agnus-castus **L. (Lamiaceae) is a medicinal plant historically used throughout the Mediterranean region to treat menstrual cycle disorders, and is still used today as a clinically effective treatment for premenstrual syndrome. The pharmaceutical activity of the plant extract is linked to its ability to lower prolactin levels. This feature has been attributed to the presence of dopaminergic diterpenoids that can bind to dopamine receptors in the pituitary gland. Phytochemical analyses of *V. agnus-castus* show that it contains an enormous array of structurally related diterpenoids and, as such, holds potential as a rich source of new dopaminergic drugs. The present work investigated the localisation and biosynthesis of diterpenoids in *V. agnus-castus*. With the assistance of matrix-assisted laser desorption ionisation-mass spectrometry imaging (MALDI-MSI), diterpenoids were localised to trichomes on the surface of fruit and leaves. Analysis of a trichome-specific transcriptome database, coupled with expression studies, identified seven candidate genes involved in diterpenoid biosynthesis: three class II diterpene synthases (diTPSs); three class I diTPSs; and a cytochrome P450 (CYP). Combinatorial assays of the diTPSs resulted in the formation of a range of different diterpenes that can account for several of the backbones of bioactive diterpenoids observed in *V. agnus-castus*. The identified CYP, *Vac*CYP76BK1, was found to catalyse 16-hydroxylation of the diol-diterpene, peregrinol, to labd-13*Z*-ene-9,15,16-triol when expressed in *Saccharomyces cerevisiae*. Notably, this product is a potential intermediate in the biosynthetic pathway towards bioactive furan- and lactone-containing diterpenoids that are present in this species.**

Keywords: bioactive diterpenoid, *Vitex agnus-castus*, terpene synthase, cytochrome P450, MALDI-MS imaging, Lamiaceae.

INTRODUCTION

Plants are a rich source of bioactive compounds, with numerous species used for millennia in traditional medicines. Advances in bioassay technology coupled with modern analytical techniques have now made it relatively

straightforward to identify specific bioactivities and to pinpoint the responsible active components in medicinal plants (Wubshet *et al.*, 2016). The subsequent drug development process and (potential) wide-scale use of any identified compounds requires a reliable and scalable source of material that is both ethically and commercially viable. This requirement is often not met by the natural plant source due to difficulties with cultivation, endangered wild populations and the inherent chemical complexity found in most medicinal plant species. While chemical synthesis can potentially provide a solution to this problem, the large number of stereocenters present in natural products makes this route challenging technically and economically. Another approach to solving this problem is via the engineering of microbial organisms to produce specific natural products using biosynthetic pathways reconstructed from the original or even a combination of plant species. Examples using *Saccharomyces cerevisiae* as a host to make important plant-derived pharmaceuticals and nutraceuticals are already available, and include: artemisinic acid, a precursor of the anti-malarial drug artimisinin, naturally produced by the plant *Artemisia annua* (Paddon *et al.*, 2013); the antioxidant compound carnosic acid from *Rosmarinus officinalis* (Ignea *et al.*, 2016; Scheler *et al.*, 2016); and the cAMP booster, forskolin, from *Coleus forskohlii* (Pateraki *et al.*, 2017). Through metabolic engineering of host organisms, routes to specific compounds can be optimised to increase yields and the generation of further chemical diversity explored through the application of combinatorial techniques (Ignea *et al.*, 2015; Andersen-Ranberg *et al.*, 2016; Jia *et al.*, 2016). For such an approach to work, the enzymes involved in the biosynthesis of a given compound are required, and this has spurred interest in biosynthetic pathway discovery in medicinal plants.

The present work focuses on diterpenoid pathway discovery in *Vitex agnus-castus* L. (Lamiaceae), a shrub that grows throughout the Mediterranean region and parts of Asia. It has a long history of use in the treatment of female reproductive conditions, and is still used today to treat premenstrual syndrome (PMS). The efficacy of crude fruit extracts for relieving symptoms of PMS and related syndromes is strongly supported by evidence from multiple clinical trials (Schellenberg, 2001; Atmaca *et al.*, 2003; He *et al.*, 2009), and include relief from latent hyperprolactinemia and cyclic mastalgia (Kilicdag *et al.*, 2004; Carmichael, 2008). In addition, extracts are considered to be safe and better tolerated than conventional hormone or selective serotonin reuptake inhibitor-based treatments (Daniele *et al.*, 2005). The pharmacological properties of *V. agnus-castus* are attributed to the presence of dopamine, opioid and oestrogen receptor ligands that are involved in modulating hormone levels that impact PMS (Wuttke *et al.*, 2003; Webster *et al.*, 2011). Specifically, those compounds thought to be responsible for the observed prolactin-lowering effect are diterpenoids that interact with dopamine receptors in the pituitary gland (Hoberg *et al.*, 1999; Jarry *et al.*, 2006; Brattström, 2014). The ability of *V. agnus-castus* diterpenoids to interact with both D2 and D3 dopamine receptors in the brain has also flagged it as a potential source of new drugs that could treat other illnesses in which dopaminergic pathways play key roles (Brattström, 2014).

A large variety of labdane-related diterpenoids has been isolated from the *Vitex* genus, with a recent review listing 114 unique structures covering a range of classes, including labdanes, abietanes and clerodanes (Yao *et al.*, 2016). The majority of diterpenoids isolated from *V. agnus-castus* incorporate hydroxyl groups at C-9 and C-13 (Figure 1a; Hoberg *et al.*, 1999; Ono *et al.*, 2008, 2009, 2011). Common structural features of *V. agnus-castus* bioactive diterpenoids are the presence of furan, lactone or 3-hydroxy-3-methyl-pent-4-enyl groups (König, 2014). Furan or lactone groups, in particular, are frequent features of bioactive diterpenoids and appear, in some cases, to be important for their activity (Lim *et al.*, 2012; Shul'ts *et al.*, 2014). For example, work on elucidating the pharmacophore of salvinorin A, indicates that the furan ring influences its kappa opioid receptor agonist activity (Munro *et al.*, 2005; Riley *et al.*, 2014). Because of their potential pharmaceutical applications, the elucidation of biosynthetic pathways towards furan and lactone diterpenoids is of particular interest (Zerbe *et al.*, 2014; Pelot *et al.*, 2017).

Terpene biosynthesis is carried out in plants by a family of related enzymes known as terpene synthases (TPSs). These divide into subfamilies based on phylogenetic relationships, with some degree of functional conservation (Bohlmann *et al.*, 1998; Chen *et al.*, 2011). In angiosperms, the core structure of labdane-related diterpenoids is typically formed from geranylgeranyl diphosphate (GGPP) via the sequential action of two diterpene synthases (diTPS; Peters, 2010). The first enzyme, a class II diTPS (TPS-c subfamily), carries out a protonation-initiated cyclisation of GGPP to generate the characteristic decalin core. The conformation of GGPP upon cyclisation – as determined by the active site of the specific class II diTPS – determines the stereochemistry of the decalin core, and this generally remains unchanged in later biosynthetic steps (Andersen-Ranberg *et al.*, 2016). It is possible for water to capture the cyclised diphosphate carbocation resulting in the introduction of a hydroxyl group (Caniard *et al.*, 2012; Zerbe *et al.*, 2014). The second enzyme, a class I diTPS (usually from the TPS-e/f subfamily), then ionises the cyclic intermediate through removal of the diphosphate group and often guides further carbocation-driven rearrangements. Again, water capture of the carbocation intermediate can occur, resulting in the introduction of a (second) hydroxyl group (Caniard *et al.*, 2012). From this scheme, the initial steps on the biosynthetic route to dopaminergic diterpenoids in

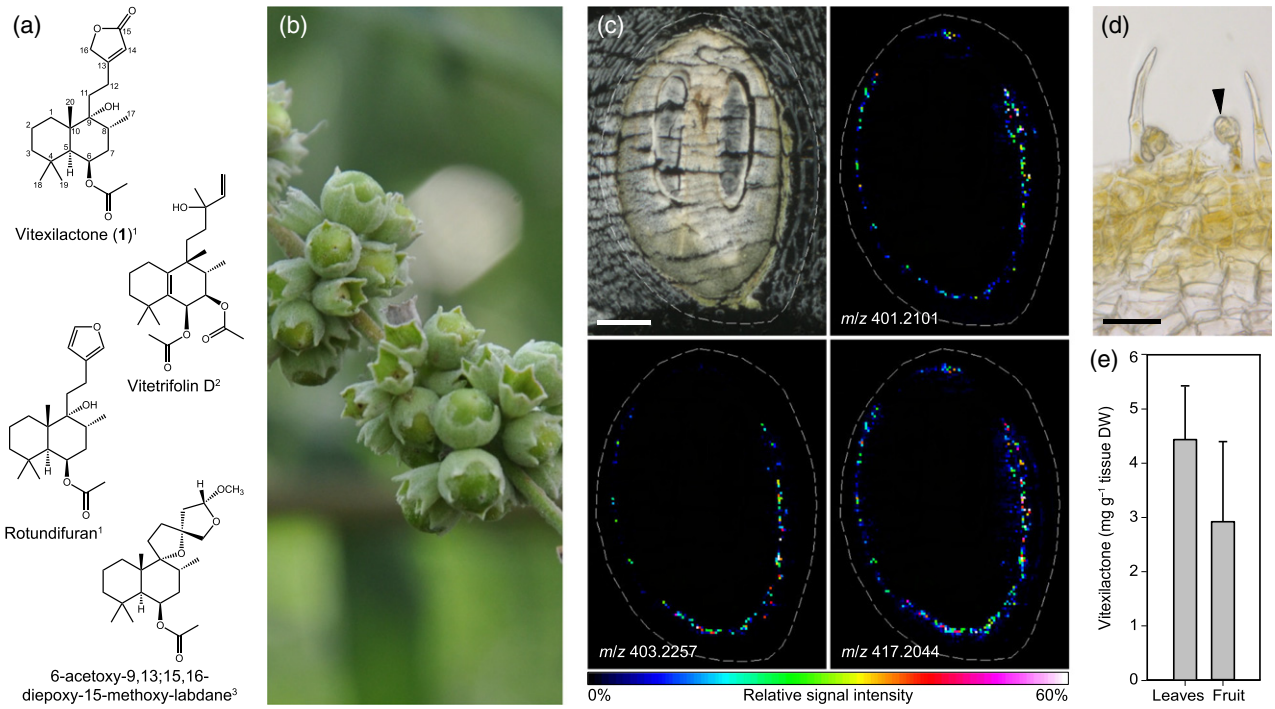

Figure 1. Metabolite profiling of *Vitex agnus-castus* tissues.
(a) Diterpenoids reported from *V. agnus-castus* fruit ([1]Hoberg *et al.*, 1999; [2]Ono *et al.*, 2011; [3]Ono *et al.*, 2009).
(b) Maturing fruit. (c) Longitudinal section through a semi-mature fruit prepared for matrix-assisted laser desorption ionisation-mass spectrometry imaging (MALDI-MSI; 1000 μm scale bar) and corresponding ion maps of co-localising *m/z* values of putative diterpenoids (see Table 1, all images TIC normalised).
(d) Bright-field image of fruit epidermis with glandular trichomes (indicated with an arrowhead, 100 μm scale bar).
(e) Quantification of vitexilactone (**1**) in leaf and fruit tissue (n = 3, error bars represent ± 1 SD). [Colour figure can be viewed at wileyonlinelibrary.com].

V. agnus-castus can be predicted to proceed via an initial class II diTPS-catalysed cyclisation of GGPP to generate bicyclic intermediates, potentially oxygenated at C-9 followed by rearrangement and dephosphorylation by a class I diTPS to yield either bi- or tricyclic labdane-related diterpenoids. Subsequent oxidative steps in the pathway towards the highly functionalised diterpenoids of *V. agnus-castus* are then likely to be carried out by members of the large cytochrome P450 (CYP) family (Ignea *et al.*, 2016; Scheler *et al.*, 2016; Pateraki *et al.*, 2017).

To identify enzymes involved in the biosynthesis of *V. agnus-castus* diterpenoids, we first localised diterpenoids to glandular trichomes on the surface of fruit and leaves with the aid of matrix-assisted laser desorption ionisation-mass spectrometry imaging (MALDI-MSI). A leaf-trichome transcriptome database was then generated and mined for candidate diTPSs and CYPs. Functional characterisation of the identified diTPSs resulted in the discovery of two diTPS combinations capable of producing a series of C-9 hydroxylated diterpenes. A CYP with high relative expression levels in trichomes was also characterised and found to hydroxylate the diol-diterpenoid, peregrinol, to yield labd-13*Z*-ene-9,15,16-triol, a potential intermediate in the biosynthetic pathway towards bioactive diterpenoids with lactone and furan groups.

RESULTS AND DISCUSSION

Tissue-specific localisation of diterpenoids in *Vitex agnus-castus*

Terpenoids often accumulate in plant tissues at or near their site of biosynthesis. This tendency has been exploited in biosynthetic pathway discovery efforts as a way to indirectly find tissues enriched in transcripts of relevant genes that can then be targeted for transcriptomics (Trikka *et al.*, 2015; Luo *et al.*, 2016; Pateraki *et al.*, 2017). Consequently, as a first step towards diterpenoid pathway discovery in *V. agnus-castus*, we focused our investigation on the metabolite profile and localisation of diterpenoids in fruit – the part of the plant traditionally used for treating PMS (Figure 1b). To determine if diterpenoids are localised to specific tissues within fruit, MALDI-MSI was used to map the spatial distribution of metabolites across longitudinal sections (Figure 1c). This technique has been used to localise diverse specialised metabolites in plant tissues (for a comprehensive review, see Boughton *et al.*, 2015), including terpenoids in the medicinal plants *Tripterygium wilfordii* (Lange *et al.*, 2017) and *Salvia divinorum* (Chen *et al.*, 2017).

Analysis of fruit sections revealed the presence of many compounds at the outer edge of the fruit with predicted

formulae consistent with diterpenoids previously reported from this species (Figure 1c; Table 1). Their observed distribution was found to overlap with that of glandular trichomes (Figure 1d), which were subsequently isolated, extracted and analysed by liquid chromatography-high-resolution mass spectrometry (LC-HRMS) to test for the presence of diterpenoids. Co-elution with a standard confirmed one of the major peaks to be vitexilactone (**1**), a labdane-type diterpenoid with a five-membered lactone ring, and of interest for its potential bioactivity (Figure 1a; Meier *et al.*, 2000). A lack of other available reference compounds and databases precluded the assignment of other peaks to specific diterpenoids. However, in the LC-HRMS analysis of trichome extracts, Na^+ adducts were observed that corresponded to the $[M + K]^+$ ions of the putative diterpenoids found to co-localise in the MALDI-MSI analysis (Table 1). In many cases, ions with the same mass were detected at multiple retention times. This can be explained by the presence of more than one compound with the same formula, which, for *Vitex* spp., could be expected given the multiple structural and stereoisomers reported in the literature for diterpenoids (Yao *et al.*, 2016).

Liquid chromatography-HRMS analysis of leaf extracts demonstrated that leaves have a very similar diterpenoid profile to fruit and, additionally, contain a comparable level of vitexilactone on a dry weight (DW) basis [with an average value ($\pm$ SD) of 4.4 ± 1.0 mg g^{-1} DW in leaves compared with 2.9 ± 1.5 mg g^{-1} DW in fruit; Figure 1e; Table 1]. Isolation and analysis of glandular trichomes from leaves showed that, as for fruit, diterpenoids are also present in these structures (Table 1). The predicted formulae of ions detected in the trichome extracts suggest diterpenoids ranging in structural complexity from simple to more complex oxidised and acetylated compounds. Some of these simple diterpenoids may represent pathway intermediates, and their presence in trichomes along with more functionalised forms supports the idea that trichomes are a site of both biosynthesis and storage. The localisation of diterpenoids to glandular trichomes is consistent with findings from other Lamiaceae species, including *R. officinalis*, *Marrubium vulgare* and *S. divinorum.* In trichomes of these species, both diterpenoid accumulation and high expression levels of relevant pathway enzymes have been reported (Brückner *et al.*, 2014; Zerbe *et al.*, 2014; Scheler *et al.*, 2016; Chen *et al.*, 2017; Pelot *et al.*, 2017).

Generation of a *Vitex agnus-castus* leaf-trichome transcriptome and identification of candidate diTPSs

Taking into consideration metabolite accumulation patterns, as well as fresh tissue availability, RNA samples from isolated leaf trichomes and whole leaves were sequenced using Illumina HiSeq technology. Reads from the two samples were *de novo* assembled using the Trinity pipeline (Haas *et al.*, 2013). Homology searches of the transcriptome databases using characterised plant diTPSs as queries resulted in the identification of six full-length transcripts. Phylogenetic analysis of the translated coding sequences revealed that *Vac*TPS1, *Vac*TPS3 and *Vac*TPS5 are members of the angiosperm class II diTPS clade assigned as TPS-c (Figure 2a; Chen *et al.*, 2011). *Vac*TPS1 and *Vac*TPS3 clustered with other Lamiaceae diTPSs from specialised metabolism: *Vac*TPS1 was most closely related to a peregrinol diphosphate synthase from *M. vulgare* (*Mv*CPS1; Zerbe *et al.*, 2014) with which it shares 61% sequence identity at the amino acid level, while *Vac*TPS3 was placed sister to this clade. In contrast, *Vac*TPS5 clustered in a clade of diTPSs with mixed activities, including *ent*-copalyl diphosphate synthases (*ent*-CPS) involved in the biosynthesis of gibberellins, but also several diTPSs involved in specialised metabolism. The most closely related diTPSs were an *ent*-CPS speculated to be involved in specialised metabolism from *Isodon eriocalyx* (IeCPS2; Li *et al.*, 2012) and a (–)-kolavenyl diphosphate synthase from *S. divinorum* (*Sd*KPS; Chen *et al.*, 2017; Pelot *et al.*, 2017), both of which *Vac*TPS5 shares 73% sequence identity at the amino acid level. The remaining three diTPSs identified from the leaf/trichome transcriptome database clustered with other class I diTPSs from the TPS-e/f sub-family (Figure 2b). *Vac*TPS2 and *Vac*TPS6 clustered in a Lamiaceae-specific group involved in specialised metabolism. Like other members of this group, both enzymes are missing the N-terminal γ-domain, with only the $\beta\alpha$ bi-domain present (Hillwig *et al.*, 2011; Pateraki *et al.*, 2014; Zerbe *et al.*, 2014). *Vac*TPS4 was found to be most closely related to *ent*-kaurene synthases involved in gibberellin biosynthesis, sharing 78% sequence identity at the amino acid level with the closest included relative, *Mv*EKS, from *M. vulgare* (Zerbe *et al.*, 2014).

To identify terpene synthase candidates likely to be involved in trichome-specific diterpenoid metabolism, transcript levels in leaves, fruit and trichomes were quantified using quantitative real-time polymerase chain reaction (qRT-PCR). All candidates, with the exception of *Vac*TPS4, had higher transcript levels in trichomes isolated from leaves and fruit relative to whole leaves and fruit, while *Vac*TPS4 expression was similar across all tissues tested (Figure 2c).

Functional characterisation of *Vac*TPSs

Characterisation of the enzymatic activity of *Vac*TPSs was carried out using the *Nicotiana benthamiana-Agrobacterium*-mediated transient expression system (Bach *et al.*, 2014). Hexane extracts of *N. benthamiana* leaves expressing *Vac*TPSs were analysed by gas chromatography-mass spectrometry (GC-MS). Product identity was determined by nuclear magnetic resonance (NMR) and/or by comparison of product profiles with those of parallel assays of

Table 1 Ions detected by MALDI-MSI found to co-localise with vitexilactone ($[M + K]^+$ 417.2044, calculated 417.2038, 1.0 ppm error) in a fruit section of *V. agnus-castus* with associated calculated molecular formulae, and corresponding detection in LC-HRMS analyses of fruit and leaf trichome extracts as either $[M + Na]^+$ or $[M + H]^+$ ions

Observed mass MALDI-MSI (m/z)	Calculated molecular formula	Error (ppm)	Adduct	Calculated mass for $[M + Na]^+$ or $[M + H]^+$	Observed mass LC-HRMS (m/z)	Retention time (min)	Compounds reported from *Vitex* spp.
345.2204	$C_{20}H_{34}O_2$	3.8	K^+	329.2451	329.2455	16, 16.4	
347.2357	$C_{20}H_{36}O_2$	2.9	K^+	331.2607	331.2612	16.7, 17.4, 17.8	Sclareol (Eryigit *et al.*, 2015), viteagnusin C (Ono *et al.*, 2008), viteagnusin D (Ono *et al.*, 2008), peregrinol (this report)
359.1993	$C_{20}H_{32}O_3$	2.7	K^+	343.2245	343.2249	16.15, 25.2	Vitexolin A (Corlay *et al.*, 2015)
373.1789	$C_{20}H_{30}O_4$	−3.7	K^+	335.2216 $[M + H]^+$	335.2216	Common fragment ion	Vitexolide A (Corlay *et al.*, 2015), vitexolide B (Corlay *et al.*, 2015), 12-epivitexolide A (Corlay *et al.*, 2015), 12S,16S/R-dihydroxy-ent-labda-7,13-dien-15,16-olide (Nyiligira *et al.*, 2008)
375.1943	$C_{20}H_{32}O_4$	2.9	K^+	359.2193	359.2189	20.4	Vitextrifolin F (Zheng *et al.*, 2013), vitexifolin E (Ono *et al.*, 2002)
383.0543	$C_{23}H_{10}O_6$	1.81	H^+	405.0370	Not observed		
387.2308	$C_{22}H_{36}O_3$	3.0	K^+	371.2557	371.2570	17.2	Viteagnusin A (Ono *et al.*, 2008), viteagnusin B (Ono *et al.*, 2008)
399.1946	$C_{22}H_{32}O_4$	3.5	K^+	383.2193	383.2192	16.7	
401.2101	$C_{22}H_{34}O_4$	3.0	K^+	385.2349	385.2352	15.8 (F), 16.4, 17.1, 17.9, 18.5	Vitetrifolin B (Ono *et al.*, 2000), rotundifuran (Ono *et al.*, 2000)
401.2306	$C_{22}H_{34}O_5$	1.8	Na^+	401.2298	See ion 417		
403.2257	$C_{22}H_{36}O_4$	2.9	K^+	387.2506	387.2514	17.5, 18.2	Vitetrifolin E (Ono *et al.*, 2001), vitetrifolin F (Ono *et al.*, 2001)
403.0658	$C_{19}H_{14}O_{10}$	0.3	H^+	403.0659 $[M + H]^+$	Not observed		
417.2044	$C_{22}H_{34}O_5$	1.5	K^+	401.2298	401.2301	12.6	Vitexilactone (confirmed by coelution with a standard; Hoberg *et al.*, 1999)
						13.6, 14.6 (F), 16.7	Viteosin A (Alam *et al.*, 2002), previtexilactone (Kiuchi *et al.*, 2004), vitexilactone B (Zheng *et al.*, 2010), negundoin A (Zheng *et al.*, 2010), viterotulin B (Lee *et al.*, 2013)
419.2053	$C_{18}H_{36}O_8$	2.7	K^+	403.2302	Not observed		
419.2201	$C_{22}H_{36}O_5$	1.56	K^+	403.2455	403.2466	13.2, 13.8, 14, 15.1 (L), 16 (L), 16.8 (L)	Negundoin E (Zheng *et al.*, 2010)
451.2116	$C_{27}H_{30}O_6$	0.3	H^+	473.1935	Not observed		
477.4104	$C_{34}H_{52}O$	2.8	H^+	499.3910	Not observed		

Co-localisation analysis was carried out using SCiLS lab software ($P \leq 0.05$, threshold value of 0.5). Mass errors between observed LC-HRMS *m/z* values and calculated molecular formulae are < 3 ppm. Specific ions detected in only fruit or only leaf trichomes have retention times denoted by F or L, respectively, all other ions were detected in both tissues. Annotations are based on comprehensive searches of the Scifinder Scholar online chemical database for compounds with matching formulae reported from *Vitex* spp., with the exception of the component (*m/z* 401.2301) eluting at 12.6 min, which was identified as vitexilactone (**1**) by comparison to an authentic standard. Ions with the same mass were detected at different retention times, and may represent structural and stereoisomers and/or are the result of in-source fragmentation of different but related parent compounds. LC-HRMS, liquid chromatography-high-resolution mass spectrometry; MALDI-MSI, matrix-assisted laser desorption ionisation-mass spectrometry imaging.

previously characterised enzymes (details are given in Table S2).

Class II diTPSs: *Vac*TPS1, *Vac*TPS3 and *Vac*TPS5

Expression of *Vac*TPS1 alone in *N. benthamiana* resulted in a single major peak (**2**; Figure 3) with a mass spectrum and retention time matching that of peregrinol (also confirmed by NMR analysis; Table S3). When coupled with *Mv*ELS, the product profile was dominated by 9,13-epoxy-labd-14-ene (**3b**) as per the native *M. vulgare* combination of *Mv*CPS1 and *Mv*ELS (Zerbe *et al.*, 2014). Combined, these data indicate that *Vac*TPS1 is a peregrinol diphosphate synthase, and is the second example of a class II diTPS that gives rise to a C-9 hydroxylated product.

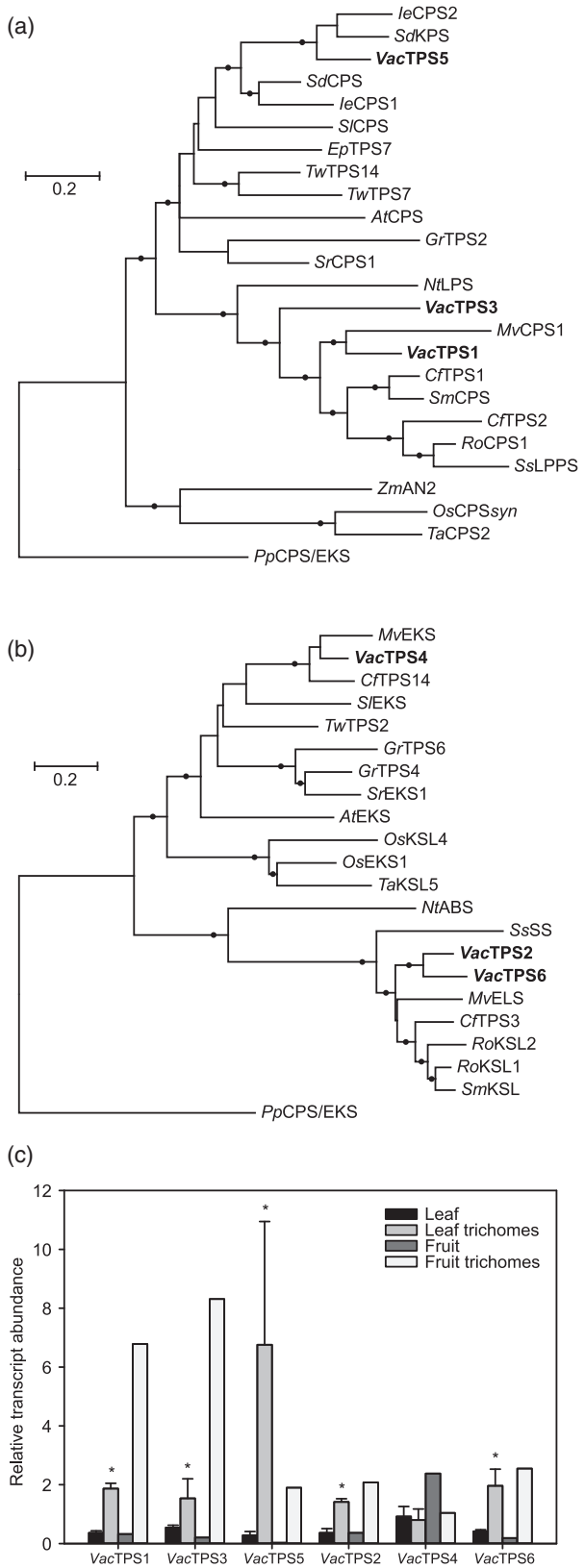

Figure 2. Phylogenetic analysis and relative transcript abundance of *Vitex agnus-castus* diterpene synthases (diTPSs).
Maximum likelihood trees of class II (a) and class I (b) diTPSs based on aligned protein sequences. Trees are drawn to scale, with branch lengths representing the number of substitutions per site. Branches with > 80% bootstrap support are indicated with a filled circle. Trees were rooted with *Pp*CPS/EKS. Genbank accession numbers are listed in Table S1.
(c) Relative transcript abundance of *V. agnus-castus* diTPSs in leaves, fruit and trichomes as determined by quantitative real-time polymerase chain reaction (qRT-PCR). For leaf data, the mean of three biological replicates (± 1 SD) is shown; for fruit, tissue was combined from three different plants to obtain sufficient trichome RNA for expression studies. Two-tailed *P*-values < 0.05 are shown with an asterisk.

Expression of *Vac*TPS3 in *N. benthamiana* resulted in a product profile matching that of a *syn*-CPS from rice, *Os*CPS*syn* (Figure 4; Xu *et al.*, 2004). Coupling of *Vac*TPS3 with a sclareol synthase from *Salvia sclarea* (*Ss*SS; Caniard *et al.*, 2012) gave the identical product profile of *Os*CPS*syn* and *Ss*SS – a single major peak corresponding to *syn*-manool/vitexifolin A (**5**; Andersen-Ranberg *et al.*, 2016; Jia *et al.*, 2016) based on retention time and mass spectrum (Figure 4). Expression of *Vac*TPS5 in *N. benthamiana* gave a product profile matching that of *Tw*TPS14, a kolavenyl diphosphate synthase characterised from *T. wilfordii* (Figure 5; Andersen-Ranberg *et al.*, 2016). Correspondingly, the coupling of *Vac*TPS5 with *Ss*SS resulted in the same product profile as the characterised coupling of *Tw*TPS14 and *Ss*SS, namely the production of the clerodane-type diterpene, kolavelool (**7**; Andersen-Ranberg *et al.*, 2016). To provide further evidence for the identity of the *Vac*TPS3 and *Vac*TPS5 products, the alcohol derivatives of the respective diphosphate products were isolated. Their structures were determined to be *syn*-copalol (**4**; Table S4) and kolavenol (**6**; Table S5) based on comparison of data from ^{1}H NMR and heteronuclear single-quantum correlation (HSQC) experiments with data from the literature (Yee and Coates, 1992; Nakano *et al.*, 2015), confirming that *Vac*TPS3 is a *syn*-CPP synthase and *Vac*TPS5 is a kolavenyl diphosphate synthase. To address the absolute configuration of the class II diTPS products, optical rotation measurements were attempted. Low quantities of isolated material did not allow for accurate calculation of the specific optical rotation; however, it should be noted that both **4** and **6** showed weak dextrorotatory (+) properties. Because the absolute configurations of the class II diphosphate derivatives, **2**, **4** and **6**, were not established, the shown structures could be either of the two possible enantiomers for each compound, with the downstream class I diTPS products expected to share the same configuration.

Class I diTPSs: *Vac*TPS2, *Vac*TPS6 and *Vac*TPS4

To characterise the activity of the three identified class I enzymes, all *V. agnus-castus* class II/class I enzyme

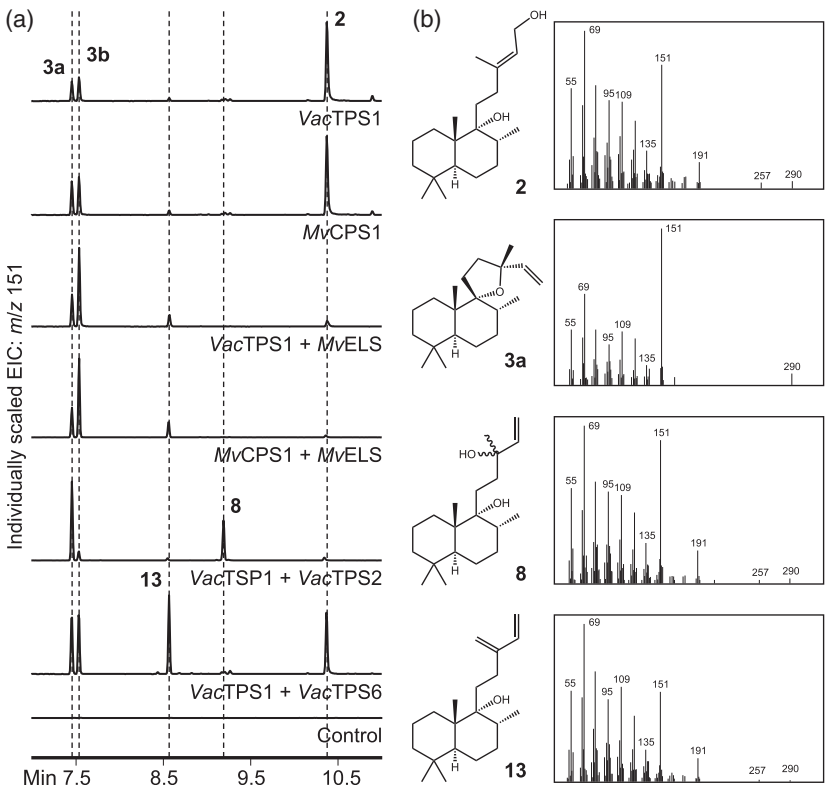

Figure 3. *In planta* functional characterisation of class II enzyme, *Vac*TPS1, and class I enzymes, *Vac*TPS2 and *Vac*TPS6.
(a) Gas chromatography-mass spectrometry (GC-MS) extracted ion chromatograms (EIC) of hexane extracts of *Nicotiana benthamiana* leaves transiently expressing combinations of diterpene synthases (diTPSs).
(b) Diterpene synthase products with representative mass spectra. Characterised diTPS combinations used as references and compound identification details are given in Table S2.

combinations were tested. Additionally, to examine the range of accepted substrates, two characterised class II diTPSs were included in the combinatorial assays: *Ep*TPS7, an *ent*-CPP synthase from *Euphorbia peplus* (Zerbe *et al.*, 2013); and *Cf*TPS2, a (+)-8-LPP synthase from *C. forskholii* (Pateraki *et al.*, 2014). Co-expression of *Vac*TPS2 with *Vac*TPS1 in *N. benthamiana* resulted in a shift in the *Vac*TPS1 product profile from **2** to two main products, **3a** and **8** (Figure 3). Structural analysis by NMR identified **3a** as 9,13(*R*)-epoxy-labd-14-ene (Table S6; presumably the C-13 epimer of **3b**) and **8** as viteagnusin D (Table S7). Derivatives of **3** are known from the *Vitex* genus (Ono *et al.*, 2008, 2009), and **8** has been isolated from fruits of *V. agnus-castus* with a series of other structurally related diterpenoids (Ono *et al.*, 2008). *Vac*TPS2 was also found to couple with *Vac*TPS3 to produce **5** – a diterpenoid previously isolated from *Vitex rotundifolia* (Figure 4; Ono *et al.*, 2002) – as per the characterised enzyme combination of *Os*CPP*syn* and *Ss*SS (Andersen-Ranberg *et al.*, 2016). A weak coupling between *Vac*TSP2 and *Vac*TPS5 to generate **7** was suggested by the presence of the characteristic *m*/*z* 257 and 189 ions at the correct retention time for this compound (when compared with the product profile of *Tw*TPS14 and *Ss*SS), but their intensity levels were too close to the background noise level for a definitive result. *Vac*TPS2 was able to accept *ent*-CPP to produce *ent*-manool (**10**) and accept (+)-8-LPP to produce 13*R*-(+)-manoyl oxide (**12a**; Figures S1 and S2). A new product was observed when *Vac*TPS6 was coupled with *Vac*TPS1, which, after isolation and structural elucidation by NMR, was identified as labda-13(16),14-dien-9-ol (**13**; Figure 3; Table S8), a recently reported diterpenoid previously only generated by an artificial combination of a bacterial enzyme, *Kg*TS, and *Mv*CPS1 (Jia *et al.*, 2016). Co-expression of *Vac*TPS6 with *Vac*TPS3 resulted in two main components identified as dehydroabietadiene (**15**) and *syn*-isopimara-7,15-diene (**14**) by comparison to the products of the characterised enzyme combination, *Os*CPP*syn* and *Cf*TPS3 (Andersen-Ranberg *et al.*, 2016). *Vac*TPS6 did not couple with *Vac*TPS5 (Figure 5), but could accept (+)-8-LPP to produce **12a** (Figure S2). *Vac*TPS4 was not found to couple with any of the *V. agnus-castus* class II enzymes or *Cf*TPS2, but when co-expressed with *Ep*TPS7 a peak corresponding to *ent*-kaurene (**16**) was observed (Figure S3). This activity would fit with a role of *Vac*TPS4 in gibberellin biosynthesis.

A complex array of diterpenoids with different labdane-related backbones is present in *V. agnus-castus* (Yao *et al.*, 2016). The molecular basis of much of this diversity can be explained by the combined activities of the class II and class I diTPSs reported here (summarised in Figure 6). The diTPSs, *Vac*TPS1, *Vac*TPS2 and *Vac*TPS6, are of particular interest as together they provide enzymatic access to C-9 hydroxylated backbones that are a feature of the bioactive preparations of this species (Jarry *et al.*, 2006). Furthermore, *Vac*TPS2 and *Vac*TPS6 display a high level of

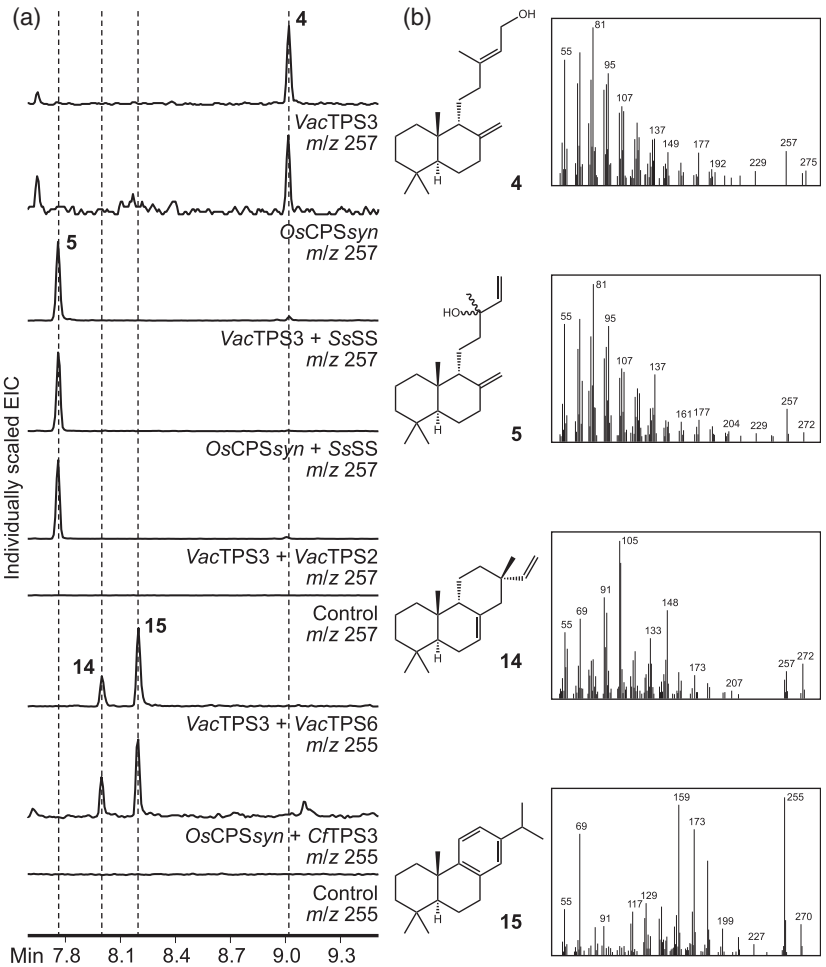

Figure 4. *In planta* functional characterisation of class II enzyme, *Vac*TPS3, and class I enzymes, *Vac*TPS2 and *Vac*TPS6.
(a) Gas chromatography-mass spectrometry (GC-MS) extracted ion chromatograms (EIC) of hexane extracts of *Nicotiana benthamiana* leaves transiently expressing combinations of diterpene synthases (diTPSs).
(b) Diterpene synthase products with representative mass spectra. Characterised diTPS combinations used as references and compound identification details are given in Table S2.

substrate promiscuity and, as such, are valuable additions to the combinatorial toolbox of class I diTPS capable of catalysing the formation of valuable diterpenoids (Andersen-Ranberg *et al.*, 2016; Jia *et al.*, 2016). Clerodane-type diterpenoids are also found in several *Vitex* species (Ono *et al.*, 2002; Lee *et al.*, 2013), and there is evidence that these may also be responsible for the dopaminergic activity observed in *V. agnus-castus* extracts (Wuttke *et al.*, 2003). Hence, the lack of a clear coupling between *Vac*TPS5 and any of the tested class I diTPSs suggests there are possibly other diTPSs not characterised in this study. A question mark also remains over the direct products of *Vac*TPS6 when supplied with *syn*-copalyl diphosphate. Dehydroabietadiene (**15**) was one of two products detected, but it is unlikely to be a direct product of *Vac*TPS6 due to a higher than usual level of oxidation. Instead, **15** is likely to be the dehydrogenated derivative of an abietane-type diterpene that has an already existing degree of unsaturation in the C-ring. Zi and Peters (2013) have demonstrated that miltiradiene easily undergoes spontaneous oxidation to **15** and, as suggested by the presence of **15** in *N. benthamiana* leaves and *S. cerevisiae* cultures expressing a levopimaradiene synthase from *Ginkgo biloba* (Matsuda and Schepmann, 2008; Brückner and Tissier, 2013), levopimaradiene can apparently also undergo a similarly facile aromatisation. In the present work no such abietane-type product was detected, and so at least one of the direct products of *Vac*TPS6 (when coupled with *Vac*TPS3) remains to be determined.

Identification of a CYP capable of peregrinol oxidation

Formation of the furan and lactone rings characteristic of bioactive *Vitex* diterpenoids is likely to be, at least in part, catalysed by the activity of CYPs. To identify possible candidate enzymes for these reactions, the transcriptome databases were searched for sequences with similarity to members of the CYP76 family – a family within the large CYP71 clan involved in the biosynthesis of specialised diterpenoids in other Lamiaceae species (Guo *et al.*, 2013; Zi and Peters, 2013; Pateraki *et al.*, 2017). A candidate gene (*Vac*CYP76BK1) was identified with high relative expression levels in leaf and fruit trichomes (Figure 7a). Phylogenetic analysis classified the candidate as the first characterised member of a new sub-family, CYP76BK,

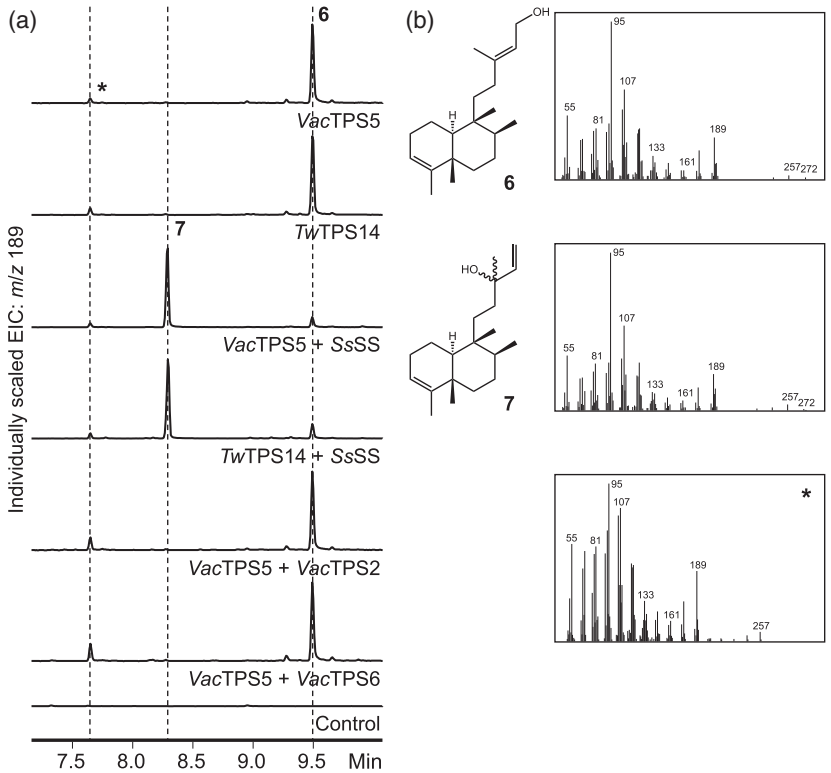

Figure 5. *In planta* functional characterisation of class II enzyme, *Vac*TPS5, and class I enzymes, *Vac*TPS2 and *Vac*TPS6.
(a) Gas chromatography-mass spectrometry (GC-MS) extracted ion chromatograms (EIC) of hexane extracts of *Nicotiana benthamiana* leaves transiently expressing combinations of diterpene synthases (diTPSs).
(b) Diterpene synthase products with representative mass spectra. Characterised diTPS combinations used as references and compound identification details are given in Table S2.

sister to the CYP76AK clade, which comprises CYPs involved in the biosynthesis of tanshinones and carnosic acid (Figure 7b; Guo *et al.*, 2016; Ignea *et al.*, 2016; Scheler *et al.*, 2016).

The ability of the identified CYP to oxygenate the C-9 hydroxylated backbones produced by the characterised *Vac*TPSs was tested using *in vitro* microsomal assays. The microsomal fraction of a *S. cerevisiae* strain expressing *Vac*CYP76BK1 [along with a cytochrome P450 reductase (CPR) from poplar; Ro *et al.*, 2002] was isolated and incubated with **2**, **3a**, **8** or **13**. LC-HRMS analysis of assays incubated with **2** revealed the presence of a new component (**17**) with an $[M + Na]^+$ ion of *m/z* 347.2558, which suggested the molecular formula $C_{20}H_{36}O_3$ (calculated $[M + Na]^+$ *m/z* 347.2557, −0.04 ppm difference; Figure 7c). No new components were observed in assays incubated with **3a**, **8** or **13** compared with control assays (Figure S4a). To confirm the activity of *Vac*CYP76BK1 *in vivo* and to obtain sufficient amounts of **17** for structural elucidation, *Vac*TPS1, *Ss*SS (previously shown in Jia *et al.*, 2016 to catalyse the formation of **8** from peregrinol diphosphate), *Vac*CYP76BK1 and a CPR from *C. forskohlii* (Pateraki *et al.*, 2017) were integrated into the genome of *S. cerevisiae* (Jensen *et al.*, 2013). Analysis of culture extracts by LC-HRMS showed production of **2**, **8** and **17** (along with additional minor components only observed when *Vac*CYP76BK1 was present; Figure 7c). **17** was isolated from an ethyl acetate extract of an engineered *S. cerevisiae* culture using a combination of silica chromatography and reversed-phase-thin-layer chromatography (RP-TLC). The structure of **17** was determined by NMR analysis to be labd-13*Z*-ene-9,15,16-triol (Table S10), a known diterpenoid isolated from another species belonging to the Lamiaceae family, *Leucas stelligera* (Kulkarni *et al.*, 2013). **17** was also found in the present study in fruit and leaf trichome extracts, along with **2**, **8** and an unidentified diterpenoid produced by *S. cerevisiae* strains expressing the diTPSs (Figure S4b and c).

That **2** appears to be a substrate for *Vac*CYP76BK1 is interesting considering it is the simple dephosphorylated form of peregrinol diphosphate, the product of the class II enzyme, *Vac*TPS1. From our experimental data it could not be determined if either of the characterised class I diTPSs are involved in its formation. **2** was observed in extracts of *N. benthamiana* leaves transiently expressing *Vac*TPS1 both with and without co-expression of class I diTPSs. The non-quantitative nature of the expression system made it difficult to determine whether either *Vac*TPS2 or *Vac*TPS6 possess simple phosphatase activity (alongside their other characterised activities) or whether the presence of **2** in these assays was due to the activity of endogenous phosphatases in *N. benthamiana*, an activity previously observed in this expression system (Andersen-Ranberg *et al.*, 2016).

Without direct evidence for the function of *Vac*CYP76BK1 in *V. agnus-castus*, we can only speculate that C-16

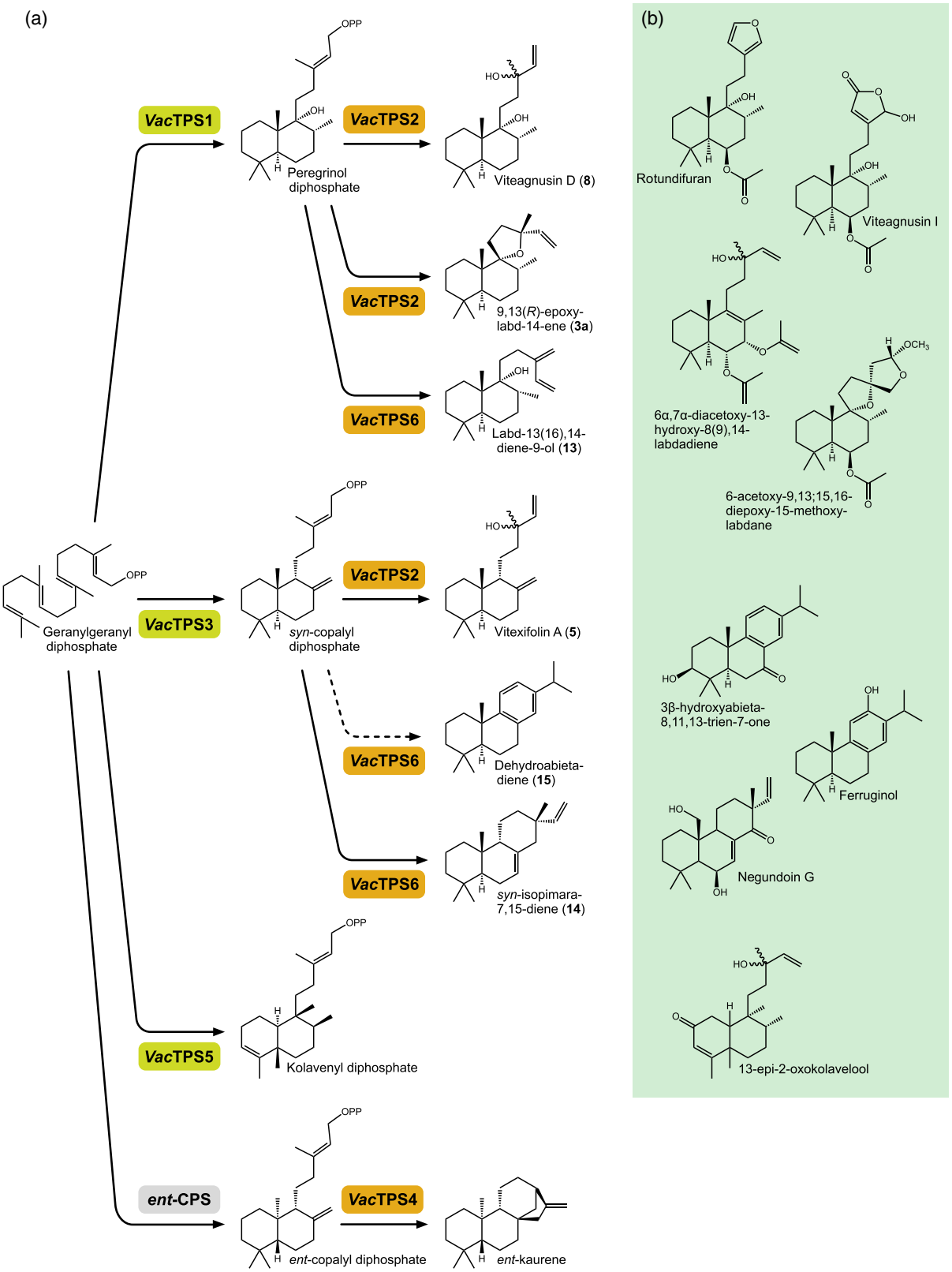

Figure 6. Summary of identified *Vitex agnus-castus* diterpene synthase (diTPS) activities.
(a) Observed enzymatic activities of *V. agnus-castus* diTPSs. Dashed arrow indicates **15** may not be the direct product of *Vac*TPS6.
(b) Examples of functionalised diterpenoids from *Vitex* spp. representing the different diterpene backbones generated by the class II and class I diTPS combinations.
[Colour figure can be viewed at wileyonlinelibrary.com].

hydroxylation of **2** is a native function of the enzyme *in planta*. Nevertheless, *Vac*CYP76BK1 was found to be expressed in the same tissue where **2** was detected, indicating that this diterpenoid would likely be available as a substrate. The addition of a hydroxyl group at this specific position of **2** to yield **17** could be considered a step towards the formation of both the lactone and furan rings characteristic of diterpenoids present in *V. agnus-castus* (Figure 1a). Further oxidation at either C-15 or C-16 of **17** to form a carboxylic acid has the potential to lead to formation of a lactone by spontaneous cyclisation (Figure 8). A similar pathway has been demonstrated for the biosynthesis of costunolide – a sesquiterpene lactone found in several Asteraceae species. Here, the C-13 methyl of the sesquiterpene backbone, germacrene A, is successively oxidised to a carboxylic acid via an aldehyde by a single CYP (de Kraker *et al.*, 2001). Hydroxylation of the nearby C-6 by a second CYP then leads to spontaneous cyclisation, resulting in lactone formation (de Kraker *et al.*, 2002; Liu *et al.*, 2011). In the case of artemisinic acid biosynthesis, an alcohol dehydrogenase and an aldehyde dehydrogenase are responsible for catalysing these steps from the sesquiterpene alcohol to the acid (Teoh *et al.*, 2009; Paddon *et al.*, 2013). A route to furan ring formation from **17** is also feasible via the aldehyde intermediate involved in lactone ring formation. In this scheme, tautomerisation of the aldehyde in a keto-enol equilibrium reaction followed by simple dehydration would afford the furan ring (Figure 8). Alternative routes to furan formation have been proposed, and involve the formation and subsequent loss of a 9,13-epoxy bridge in conjunction with an additional oxidation of C-15 or C-16 (Henderson and McCrindle, 1969; Zerbe *et al.*, 2014). It seems, however, that the presence of the C-9 hydroxyl (and by extension the 9,13-epoxy bridge) is not essential for furan or lactone ring formation as multiple furan- and lactone-bearing diterpenoids without C-9 hydroxylation exist (Smith *et al.*, 1982; Omosa *et al.*, 2014; Anwar *et al.*, 2017). Nevertheless, a potential intermediate of this alternative route was identified in the present study as a major product of *Vac*TPS2 when coupled with *Vac*TPS1 (**3a**), and similar compounds are often encountered in other furan/lactone diterpenoid-producing species (Ono *et al.*, 1999; Tesso and König, 2004; Kulkarni *et al.*, 2013). The sheer number of structurally related diterpenoids

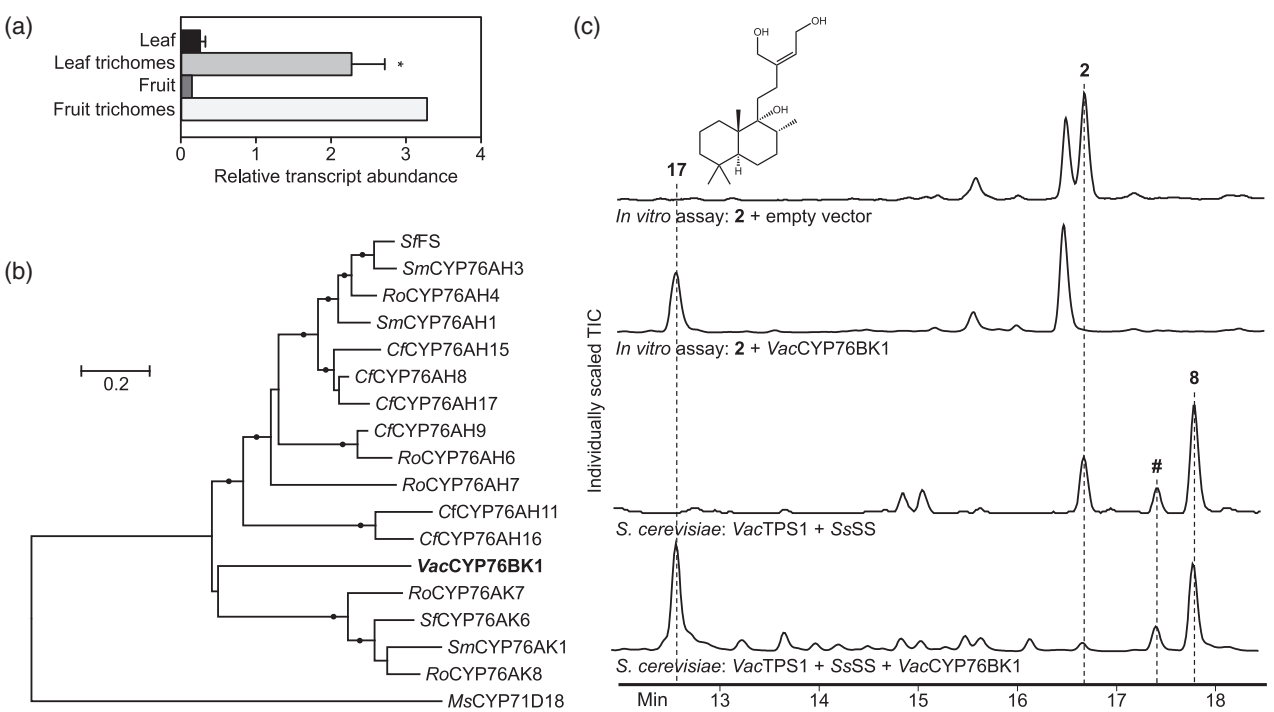

Figure 7. Phylogenetic analysis, relative transcript abundance in *Vitex agnus-castus* tissues and activity of *Vac*CYP76BK1.
(a) Relative transcript abundance of *Vac*CYP76BK1 in leaves, fruit and trichomes as determined by quantitative real-time polymerase chain reaction (qRT-PCR). For leaf data, the mean of three biological replicates (± 1 SD) is shown; for fruit, tissue was combined from three different plants to obtain sufficient trichome RNA for expression studies. Two-tailed *P*-values < 0.05 are shown with an asterisk.
(b) Maximum Likelihood tree of cytochrome P450s (CYPs) based on aligned protein sequences. The tree is drawn to scale, with branch lengths representing substitutions per site. Branches with > 80% bootstrap support are indicated with a filled circle. The tree was rooted with *Ms*CYP71D18. Genbank accession numbers are listed in Table S9.
(c) Liquid chromatography-high-resolution mass spectrometry (LC-HRMS) total ion chromatograms of microsomal assay extracts prepared from a *Saccharomyces cerevisiae* strain expressing *Vac*CYP76BK1 supplied with peregrinol (**2**), and culture extracts of *S. cerevisiae* strains expressing either diterpene synthases (diTPSs) alone or in combination with *Vac*CYP76BK1.

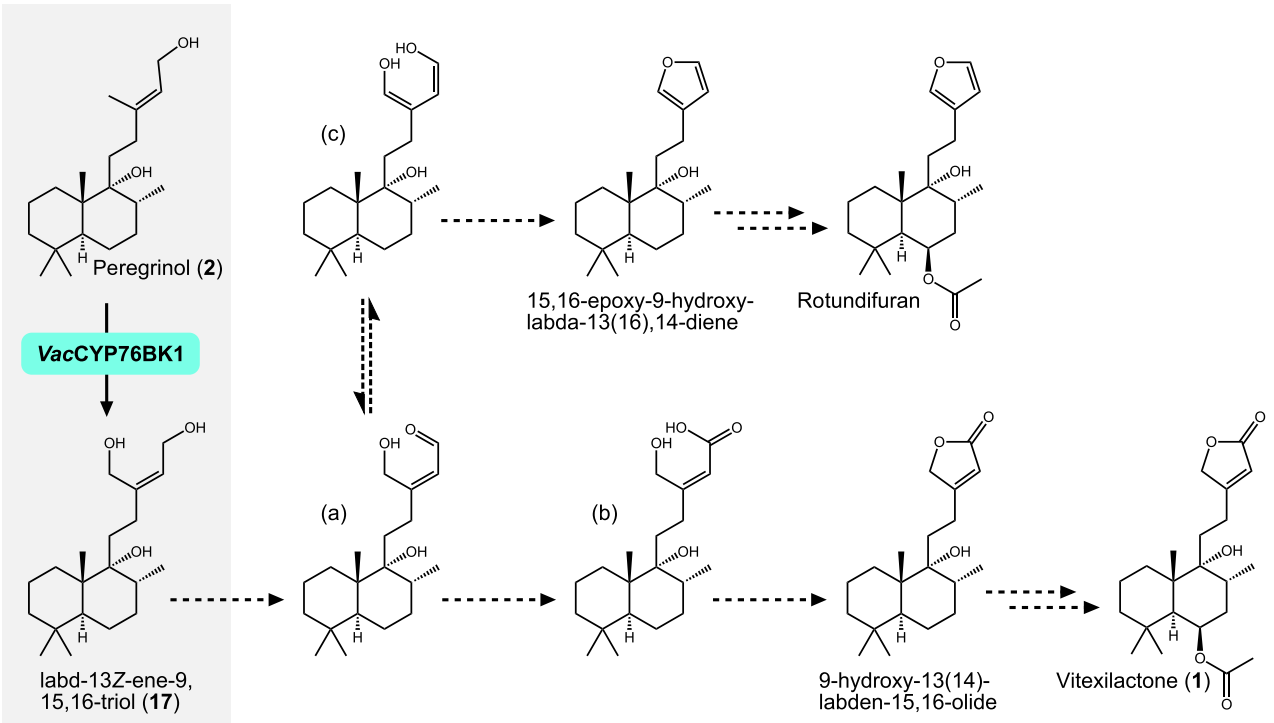

Figure 8. Proposed pathway for the formation of lactone and furan derivatives of peregrinol (**2**) via labd-13*Z*-ene-9,15,16-triol (**17**).
Lactone formation could proceed from **17** via a dehydrogenase catalysed oxidation giving rise to an aldehyde (a) and to a carboxylic acid (b), followed by an enzyme catalysed or spontaneous dehydration reaction to form the lactone ring. Alternatively, dehydration of the tautomeric enol form (c) of the aldehyde intermediate (a) would afford furan ring formation. Dashed arrows indicate putative steps. [Colour figure can be viewed at wileyonlinelibrary.com].

found in *V. agnus-castus* points to the existence of a complex metabolic grid comprised of (multifunctional) enzymes, which combine to generate the observed chemical diversity. In such a system, multiple routes to furan and lactone diterpenoids may exist.

In the present work, we have described the functional characterisation of a family of diTPSs in *V. agnus-castus*. Combined, the diTPSs could generate a range of diterpene backbones that form the biosynthetic basis for the multitude of highly functionalised labdane- and clerodane-type diterpenoids observed in this species. Several of these functionalised diterpenoids possess unique therapeutic properties, and the described CYP offers a potential enzymatic step towards their biosynthesis. Our findings accordingly show how *V. agnus-castus* offers a valuable source of enzymes that can be implemented in the engineering of biosynthetic pathways for the production of high-value diterpenoids.

EXPERIMENTAL PROCEDURES

Plant material

Vitex agnus-castus seeds were obtained from a plant growing in a private garden in Chania (Crete, Greece), and were germinated and grown in the greenhouse at the University of Copenhagen, Denmark (minimum day length/temperature: 11 h/12°C). Samples of leaves and semi-mature fruit were harvested from three individual plants. Tissues were ground in liquid nitrogen and stored at −80°C until use or prepared for MALDI-MSI (see below).

MALDI-MSI and sample preparation

Vitex agnus-castus fruit were embedded in denatured albumin (boiled egg-white) and frozen over a bath of liquid nitrogen. Albumin embedded fruit were cryosectioned (Leica CM3050 S cryostat, Leica Microsystems, Wetzler, Germany) and sections gently pressed onto pre-chilled double-sided carbon tape attached to glass slides. Slides were freeze-dried overnight and stored in a vacuum desiccator. 2,5-Dihydroxybenzoic acid was used as matrix and sublimed onto tissue sections using a custom-built sublimation apparatus at temperatures of 130–140°C at vacuum pressures of <0.1 mbar for a period of 4–6 min. A Bruker SolariX 7 XR Tesla Hybrid ESI/MALDI-FT-ICR-MS (Bruker Daltonik, Bremen, Germany) was used to acquire MS images. For data acquisition and analysis details, see Data S1.

Metabolite analysis

For metabolite analyses, ground *V. agnus-castus* tissues were extracted with n-hexane or acetonitrile with shaking incubation at 25°C for 1 h. Hexane samples were analysed by GC-MS using a Shimadzu GCMS-QP2010 Ultra (Shimadzu, Kyoto, Japan) with an HP-5MS UI column (20 m × 0.18 mm i.d., 0.25 μm film thickness; Agilent, Santa Clara, CA, USA) with H_2 as the carrier gas. The injection port was operated in splitless mode at 250°C, and the GC

program was as follows: 60°C for 1 min, ramp to 150°C at 30°C min^{-1}, ramp to 250°C at 15°C min^{-1}, ramp to 290°C at 30°C min^{-1}, hold for 3 min. The MS used electron impact (EI) ionisation with the ion source voltage and temperature set to 70 eV and 300°C, respectively. The programmed temperature vaporisation method (PTV) was used to analyse *Vac*TPS1 products due to known degradation issues with peregrinol-type diterpenoids (Zerbe *et al.*, 2014). Here initial injection port temperature was held at 40°C for 1 min, then ramped to 250°C over 4 min. LC-HRMS analyses of acetonitrile extracts were performed using the coupled Ultimate 3000 UHPLC+ Focused system (Dionex, Sunnyvale, CA, USA) and Bruker Compact ESI-QTOF-MS (Bruker) system described in Pateraki *et al.* (2017) with the following gradient method: 0–1 min, 20% B; 1–23 min, 20–100% B; 23–25 min, 100%; 25–25.5 min, 100–120%; 25.5–30.5 min, 20% B. Mass spectra were acquired in positive ion mode with the following ESI settings: capillary voltage, 4000 V; end plate offset, –500 V; dry gas temperature, 220°C; dry gas flow of 8 L min^{-1}; nebuliser pressure, 2 bar. Data were analysed using DataAnalysis 4.1 (Bruker).

Quantification of vitexilactone

Quantification of vitexilactone was carried out on diluted acetonitrile extracts by LC-MS/MS using an external standard curve of vitexilactone. For details see, Data S1.

Transcriptome sequencing and assembly

Vitex agnus-castus leaf total RNA was extracted from expanding leaves using the Spectrum Plant Total RNA Kit (Sigma-Aldrich, St Louis, MO, USA). RNA was also extracted from a trichome-enriched leaf tissue sample achieved by shaking leaves in a dry-ice-filled 50-ml tube. Trichomes adhered to the tube walls along with some broken leaf material were washed off with lysis buffer and extracted as above. Transcriptome sequencing was carried out by Macrogen (Seoul, South Korea) on an Illumina HiSeq2000 sequencer (Illumina, San Diego, CA, USA) to generate paired-end libraries (2 × 100 bp). The reads were *de novo* assembled and relative transcript abundance estimated using the Trinity pipeline (Haas *et al.*, 2013).

Phylogenetic analysis

Amino acid sequences from *V. agnus-castus* were aligned in MEGA 6.06 (Hall, 2013) with functionally characterised diTPS or CYP amino acid sequences from other plants species retrieved from GenBank (http://www.ncbi.nlm.nih.gov/; accession numbers are given in Tables S1 and S9) using MUSCLE with default settings (Edgar, 2004). The alignments were manually trimmed to remove terminal gaps and, in the case of diTPS alignments, N-terminal plastid targeting peptides were also removed. Phylogenetic trees were constructed using the Maximum Likelihood method based on the JTT matrix-based model with a site coverage cut-off of 90%. To model evolutionary rate differences among sites, a discrete Gamma distribution was used with five categories. Trees are drawn to scale, with branch lengths representing the number of substitutions per site. Trees were tested by bootstrapping with 1000 repetitions. The class I and class II diTPS trees were rooted with PpCPS/EKS from *Physcomitrella patens*, and the CYP tree was rooted with CYP71D18 from *Mentha spicata*.

RNA extraction and qRT-PCR

RNA was extracted from whole leaves, fruit and trichomes (isolated by brushing the surface of frozen tissue samples) using the Ambion RNAqueous-Micro Total RNA Isolation Kit with Plant RNA isolation Aid (Thermo Fisher Scientific, Waltham, MA, USA) and DNAse treated using the Turbo DNA-free Kit (Thermo Fisher Scientific). Quality control of RNA samples was performed with a 2100 Bioanalyzer Instrument (Agilent). cDNA libraries were generated using an iScript cDNA Synthesis Kit (Bio-Rad Laboratories, Hercules, CA, USA). qRT-PCR reactions were performed with gene-specific primers (Table S11) and the SensiFAST SYBR® No-ROX Kit master mix (Bioline Reagents, UK) on a CFX384 Touch Real-Time PCR Detection System (Bio-Rad) using the following two-step cycling parameters: 95°C for 2 min, followed by 45 cycles of 95°C for 5 sec and then 60°C for 30 sec. Melt curve analysis was performed by increasing the temperature from 65°C to 95°C in 0.5°C increments. RNA polymerase II subunit 3 was used as the reference gene. Gene expression levels were calculated using the efficiency corrected delta Ct (EΔ-Ct) method with the specific efficiency (E) of each primer pair calculated using a standard curve based on four log dilutions of cDNA template. All reactions were carried out in three technical replicates, and values reported for leaves and leaf trichomes are the mean of three biological replicates. For fruit trichomes tissue was pooled from three different plants to obtain sufficient trichome RNA for expression studies. A Student's *t*-test was used to test for statistically significant differences in gene expression levels between leaves and leaf trichomes using SigmaPlot 13.0 (Systat Software, San Jose, CA, USA).

Cloning and transient expression of candidate genes from *Vitex agnus-castus* in *Nicotiana benthamiana*

Candidates were amplified with gene-specific primers (Table S11) from cDNA generated from leaf trichome total RNA using SuperScript III First-Strand Synthesis System for RT-PCR (Invitrogen, Carlsbad, CA, USA). The cloning procedure and transient expression of TPSs in *N. benthamiana* was performed as described in Andersen-Ranberg *et al.* (2016). Five–seven days after infiltration, leaf discs were extracted and analysed by GC-MS as per 'Metabolite analysis'. Characterised diTPSs used in the reference assays were provided by Johan Andersen-Ranberg (University of Copenhagen) in pCAMBIA130035Su.

Microsome preparation and *in vitro* assays

The *S. cerevisiae* strain AM94 (Ignea *et al.*, 2012) was transformed with the expression vectors pYX143 carrying the poplar CYP reductase, CPR2 (Ro *et al.*, 2002), under the control of the ADH1 promoter and either PYeDP60 carrying *Vac*CYP76BK1 under the control of the GAL10-CYC1 promoter or without the insert (empty vector) as control. Transformants were grown for 24 h at 30°C and 110 rpm in 50 ml of synthetic complete (SC) selection media (minus leucine and uracil) with 2% glucose. The cells were pelleted and resuspended in 200 ml SC selection media with 2% galactose and grown for a further 24 h. Microsomes were prepared as described in Pompon *et al.* (1996), and *in vitro* assays performed as described in Hamann and Møller (2007).

Saccharomyces cerevisiae strain construction and testing

The *S. cerevisiae* strains were constructed and grown for metabolite analysis as described in Andersen-Ranberg *et al.* (2016). Codon optimised *Vac*TPS1 and *Ss*SS (GeneArt, Thermo Fisher Scientific) were used to generate **2** and also viteagnusin D (**8**) (Jia *et al.*, 2016), and were cloned into *S. cerevisiae* genome integration plasmids for integration into the XI-5 locus along with codon optimised *Vac*CYP76BK1 and *Cf*CPR (Pateraki *et al.*, 2017). *Vac*TPS1 and *Ss*SS (Caniard *et al.*, 2012) were under the control of

the TEF1 and PGK1 promoters, respectively, *Vac*CYP76BK1 was under the control of the TDH3 promoter, and *Cf*CPR was under the control of the TEF2 promoter. For metabolite analysis of transformants, culture aliquots of 200 μl were extracted with an equal volume of ethyl acetate (EtOAc), vortexed and centrifuged. The EtOAc layer was dried under N_2, re-suspended in 150 μl acetonitrile and analysed by LC-HRMS as per 'Metabolite analysis'.

Compound isolation and NMR experiments

For details, see Data S1.

ACCESSION NUMBERS

Nucleotide sequences reported in this study were submitted to the National Center for Biotechnology Information (NCBI) GenBankTM/EBI Data Bank with accession numbers: *Vac*TSP1, MG696748; *Vac*TSP2, MG696749; *Vac*TSP3, MG696750; *Vac*TSP4, MG696751; *Vac*TSP5, MG696752; *Vac*TSP6, MG696753; *Vac*CYP76BK1, MG696754.

ACKNOWLEDGEMENTS

The authors thank Dan Luo and Qing Liu for assistance with microsomal assays, Codruta Ignea for AM94 *S. cerevisiae* strain, and the greenhouse personnel, specifically Theodor Emil Bolsterli, at the University of Copenhagen for growing and caring for their plants. The authors gratefully acknowledge Dr David Nelson (University of Tennessee) for CYP naming. This work was supported by the Center for Synthetic Biology (University of Copenhagen Excellence Program for Interdisciplinary Research), by a European Research Council Advanced Grant to BLM (ERC-2012-ADG_20120314), and by the Danish Innovation Foundation funded project 'Plant Power: light-driven synthesis of complex terpenoids using cytochrome P450s' (12-131834; project lead, Dr Poul Erik Jensen, University of Copenhagen). AMH was supported by a Marie Skłodowska Curie Individual Fellowship. TCMS was supported by a SLAI grant from the Ministry of Higher Education Malaysia. MALDI-MSI was conducted at Metabolomics Australia (School of BioSciences, The University of Melbourne, Australia), a NCRIS initiative under Bioplatforms Australia Pty Ltd. The authors declare no competing financial interests.

SUPPORTING INFORMATION

Additional Supporting Information may be found in the online version of this article.

Figure S1. *In planta* assays of class I enzymes *Vac*TPS2 and *Vac*TPS6 with a class II *ent*-copalyl diphosphate synthase from *Euphorbia peplus* (*Ep*TPS7).

Figure S2. *In planta* assays of class I enzymes *Vac*TPS2 and *Vac*TPS6 with a class II labd-13-en-8-ol diphosphate synthase from *Coleus forskohlii* (*Cf*TPS2).

Figure S3. *In planta* assays of class I enzyme *Vac*TPS4.

Figure S4. (a) LC-HRMS total ion chromatograms of microsomal assay extracts. (b) and (c) LC-HRMS extracted ion chromatograms (EIC) comparing the product profile of the *Vac*CYP76BK1 expressing *S. cerevisiae* strain with *V. agnus-castus* leaf and fruit trichome extracts.

Table S1. Genes used in the diTPS phylogenetic analysis.

Table S2. Compounds reported in this paper and the method of identification.

Table S3. Peregrinol (**2**) NMR data.

Table S4. *syn*-Copalol (**4**) NMR data.

Table S5. Kolavenol NMR data.

Table S6. 9,13-Epoxy-labd-14-ene (**3a**) NMR data.

Table S7. Viteagnusin D (**8**) NMR data.

Table S8. Labda-13(16),14-dien-9-ol (**13**)NMR data.

Table S9. Genes used in the cytochrome P450 phylogenetic analysis.

Table S10. Labd-13*Z*-ene-9,15,16-triol (**17**) NMR data.

Table S11. Primers used for isolation and cloning of *V. agnus-castus* genes, *Cf*CPR and *Ss*SS, and qRT-PCR experiments.

Data S1. Methods.

REFERENCES

Alam, G., Wahyuono, S., Ganjar, I.G., Hakim, L., Timmerman, H. and Verpoorte, R. (2002) Tracheospasmolytic activity of viteosin-A and vitexicarpin isolated from *Vitex trifolia*. *Planta Med.* **68**, 1047–1049.

Andersen-Ranberg, J., Kongstad, K.T., Nielsen, M.T. *et al.* (2016) Expanding the landscape of diterpene structural diversity through stereochemically controlled combinatorial biosynthesis. *Angewandte Chemie Int. Edn* **128**, 2182–2186.

Anwar, L., Efdi, M., Ninomiya, M. and Ibrahim, S. (2017) Labdane diterpene lactones of *Vitex pubescens* and their antileukemic properties. *Med. Chem. Res.* **26**, 2357–2362. https://doi.org/10.1007/s00044-00017-01937-00043.

Atmaca, M., Kumru, S. and Tezcan, E. (2003) Fluoxetine versus *Vitex agnus-castus* extract in the treatment of premenstrual dysphoric disorder. *Hum. Psychopharm.* **18**, 191–195.

Bach, S.S., Bassard, J.-É., Andersen-Ranberg, J., Møldrup, M.E., Simonsen, H.T. and Hamberger, B. (2014) High-throughput testing of terpenoid biosynthesis candidate genes using transient expression in *Nicotiana benthamiana*. In *Plant Isoprenoids*. (Rodríguez-Concepción, M., ed). New York: Springer, pp. 245–255.

Bohlmann, J., Meyer-Gauen, G. and Croteau, R. (1998) Plant terpenoid synthases: molecular biology and phylogenetic analysis. *Proc. Natl Acad. Sci.* **95**, 4126–4133.

Boughton, B.A., Thinagaran, D., Sarabia, D., Bacic, A. and Roessner, U. (2015) Mass spectrometry imaging for plant biology: a review. *Phytochem. Rev.* **15**, 445–488.

Brattström, A. (2014) Dopaminergic activity of *Vitex* diterpenoids. USA: Patent No. US 8,637,099 B2, 28 January 2014.

Brückner, K. and Tissier, A. (2013) High-level diterpene production by transient expression in *Nicotiana benthamiana*. *Plant Meth.* **9**, 46.

Brückner, K., Božić, D., Manzano, D., Papaefthimiou, D., Pateraki, I., Scheler, U., Ferrer, A., De Vos, R.C.H., Kanellis, A.K. and Tissier, A. (2014) Characterization of two genes for the biosynthesis of abietane-type diterpenes in rosemary (*Rosmarinus officinalis*) glandular trichomes. *Phytochemistry*, **101**, 52–64.

Caniard, A., Zerbe, P., Legrand, S., Cohade, A., Valot, N., Magnard, J.-L., Bohlmann, J. and Legendre, L. (2012) Discovery and functional characterization of two diterpene synthases for sclareol biosynthesis in *Salvia sclarea* (L.) and their relevance for perfume manufacture. *BMC Plant Biol.* **12**, 119.

Carmichael, A.R. (2008) Can *Vitex agnus-castus* be used for the treatment of mastalgia? What is the current evidence? *Evid. Comp. Alt. Med.* **5**, 247–250.

Chen, F., Tholl, D., Bohlmann, J. and Pichersky, E. (2011) The family of terpene synthases in plants: a mid-size family of genes for specialized metabolism that is highly diversified throughout the kingdom. *Plant J.* **66**, 212–229.

Chen, X., Berim, A., Dayan, F.E. and Gang, D.R. (2017) A (–)-kolavenyl diphosphate synthase catalyzes the first step of salvinorin A biosynthesis in *Salvia divinorum*. *J. Exp. Bot.* **68**, 1109–1122.

Corlay, N., Lecsö-Bornet, M., Leborgne, E., Blanchard, F., Cachet, X., Bignon, J., Roussi, F., Butel, M.J., Awang, K. and Litaudon, M. (2015) Antibacterial labdane diterpenoids from *Vitex vestita*. *J. Nat. Prod.* **78**, 1348–1356.

Daniele, C., Thompson Coon, J., Pittler, M.H. and Ernst, E. (2005) *Vitex agnus-castus*: a systematic review of adverse events. *Drug Saf.*, **28**, 319–332.

Edgar, R.C. (2004) MUSCLE: multiple sequence alignment with high accuracy and high throughput. *Nucleic Acids Res.* **32**, 1792–1797.

Eryigit, T., Çig, A., Okut, N., Yildirim, B. and Ekici, K. (2015) Evaluation of chemical composition and antimicrobial activity of *Vitex agnus-castus* L. fruits' essential oils from West Anatolia. *Turkey. J. Essen. Oil Bear. Plants*, **18**, 208–214.

Guo, J., Zhou, Y.J., Hillwig, M.L. *et al.* (2013) CYP76AH1 catalyzes turnover of miltiradiene in tanshinones biosynthesis and enables heterologous production of ferruginol in yeasts. *Proc. Natl Acad. Sci. USA* **110**, 12108–12113.

Guo, J., Ma, X., Cai, Y. *et al.* (2016) Cytochrome P450 promiscuity leads to a bifurcating biosynthetic pathway for tanshinones. *New Phytol.* **210**, 525–534.

Haas, B.J., Papanicolaou, A., Yassour, M. *et al.* (2013) De novo transcript sequence reconstruction from RNA-seq using the Trinity platform for reference generation and analysis. *Nat. Prot.* **8**, 1494–1512.

Hall, B.G. (2013) Building phylogenetic trees from molecular data with MEGA. *Mol. Biol. Evol.* **30**, 1229–1235.

Hamann, T. and Møller, B.L. (2007) Improved cloning and expression of cytochrome P450s and cytochrome P450 reductase in yeast. *Protein Expr. Purif.* **56**, 121–127.

He, Z., Chen, R., Zhou, Y., Geng, L., Zhang, Z., Chen, S., Yao, Y., Lu, J. and Lin, S. (2009) Treatment for premenstrual syndrome with *Vitex agnus castus*: a prospective, randomized, multi-center placebo controlled study in China. *Maturitas*, **63**, 99–103.

Henderson, M.S. and McCrindle, R. (1969) Premarrubiin. A diterpenoid from *Marrubium vulgare* L. *J. Chem. Soc.* 2014–2015.

Hillwig, M.L., Xu, M., Toyomasu, T., Tiernan, M.S., Wei, G., Cui, G., Huang, L. and Peters, R.J. (2011) Domain loss has independently occurred multiple times in plant terpene synthase evolution. *Plant J.* **68**, 1051–1060.

Hoberg, E., Orjala, J., Meier, B. and Sticher, O. (1999) Diterpenoids from the fruits of *Vitex agnus-castus*. *Phytochemistry*, **52**, 1555–1558.

Ignea, C., Trikka, F.A., Kourtzelis, I., Argiriou, A., Kanellis, A.K., Kampranis, S.C. and Makris, A.M. (2012) Positive genetic interactors of HMG2 identify a new set of genetic perturbations for improving sesquiterpene production in *Saccharomyces cerevisiae*. *Microb. Cell Fact.* **11**, 1–16.

Ignea, C., Ioannou, E., Georgantea, P., Loupassaki, S., Trikka, F.A., Kanellis, A.K., Makris, A.M., Roussis, V. and Kampranis, S.C. (2015) Reconstructing the chemical diversity of labdane-type diterpene biosynthesis in yeast. *Metab. Eng.* **28**, 91–103.

Ignea, C., Athanasakoglou, A., Ioannou, E., Georgantea, P., Trikka, F.A., Loupassaki, S., Roussis, V., Makris, A.M. and Kampranis, S.C. (2016) Carnosic acid biosynthesis elucidated by a synthetic biology platform. *Proc. Natl Acad. Sci. USA* **113**, 3681–3686.

Jarry, H., Spengler, B., Wuttke, W. and Christoffel, V. (2006) In vitro assays for bioactivity-guided isolation of endocrine active compounds in *Vitex agnus-castus*. *Maturitas*, **55S**, 26–36.

Jensen, N.B., Strucko, T., Kildegaard, K.R., David, F., Maury, J., Mortensen, U.H., Forster, J., Nielsen, J. and Borodina, I. (2013) EasyClone: method for iterative chromosomal integration of multiple genes in *Saccharomyces cerevisiae*. *FEMS Yeast Res.* **14**, 238–248.

Jia, M., Potter, K.C. and Peters, R.J. (2016) Extreme promiscuity of a bacterial and a plant diterpene synthase enables combinatorial biosynthesis. *Metab. Eng.* **37**, 24–34.

Kilicdag, E.B., Tarim, E., Bagis, T., Erkanli, S., Aslan, E., Ozsahin, K. and Kuscu, E. (2004) Fructus agni casti and bromocriptine for treatment of hyperprolactinemia and mastalgia. *Int. J. Gynecol. Obstet.* **85**, 292–293.

Kiuchi, F., Matsuo, K., Ito, M., Qui, T.K. and Honda, G. (2004) New norditerpenoids with trypanocidal activity from *Vitex trifolia*. *Chem. Pharmaceut. Bull.* **52**, 1492–1494.

König, S. (2014) Composition and activity of *Vitex agnus-castus*. *Biomacromol. Mass Spect.* **3**, 291–312.

de Kraker, J.W., Franssen, M.C.R., Dalm, M.C.F., de Groot, A. and Bouwmeester, H.J. (2001) Biosynthesis of germacrene A carboxylic acid in chicory roots. Demonstration of a cytochrome P450 (+)-germacrene A hydroxylase and NADP+-dependent sesquiterpenoid dehydrogenase(s) involved in sesquiterpene lactone biosynthesis. *Plant Physiol.* **125**, 1930–1940.

de Kraker, J.W., Franssen, M.C.R., Joerink, M., De Groot, A. and Bouwmeester, H.J. (2002) Biosynthesis of costunolide, dihydrocostunolide, and leucodin. Demonstration of cytochrome P450-catalyzed formation of the lactone ring present in sesquiterpene lactones of chicory. *Plant Physiol.* **129**, 257–268.

Kulkarni, R.R., Shurpali, K., Puranik, V.G., Sarkar, D. and Joshi, S.P. (2013) Antimycobacterial labdane diterpenes from *Leucas stelligera*. *J. Nat. Prod.* **76**, 1836–1841.

Lange, B.M., Fischedick, J.T., Lange, M.F., Srividya, N., Šamec, D. and Poirier, B.C. (2017) Integrative approaches for the identification and localization of specialized metabolites in *Tripterygium* roots. *Plant Physiol.* **173**, 456–469.

Lee, C., Lee, J.W., Jin, Q. *et al.* (2013) Anti-inflammatory constituents from the fruits of *Vitex rotundifolia*. *Bioorg. Med. Chem. Lett.* **23**, 6010–6014.

Li, J.L., Chen, Q.Q., Jin, Q.P., Gao, J., Zhao, P.J., Lu, S. and Zeng, Y. (2012) leCPS2 is potentially involved in the biosynthesis of pharmacologically active *Isodon* diterpenoids rather than gibberellin. *Phytochemistry*, **76**, 32–39.

Lim, J.C.W., Chan, T.K., Ng, D.S.W., Sagineedu, S.R., Stanslas, J. and Wong, W.S.F. (2012) Andrographolide and its analogues: versatile bioactive molecules for combating inflammation and cancer. *Clin. Exp. Pharmacol. Physiol.* **39**, 300–310.

Liu, Q., Majdi, M., Cankar, K., Goedbloed, M., Charnikhova, T., Verstappen, F.W.A., de Vos, R.C.H., Beekwilder, J., van der Krol, S. and Bouwmeester, H.J. (2011) Reconstitution of the costunolide biosynthetic pathway in yeast and *Nicotiana benthamiana*. *PLoS ONE* **6**, e23255.

Luo, D., Callari, R., Hamberger, B. *et al.* (2016) Oxidation and cyclization of casbene in the biosynthesis of *Euphorbia* factors from mature seeds of *Euphorbia lathyris* L. *Proc. Natl Acad. Sci. USA* **113**, E5082–E5089.

Matsuda, S.P.T. and Schepmann, H.G. (2008) *Ginkgo biloba* levopimaradiene synthase (USA ed: Patent No. US 7,374,920 B2, 20 May 2008).

Meier, B., Berger, D., Hoberg, E., Sticher, O. and Schaffner, W. (2000) Pharmacological activities of *Vitex agnus-castus* extracts in vitro. *Phytomedicine*, **7**, 373–381.

Munro, T.A., Rizzacasa, M.A., Roth, B.L., Toth, B.A. and Yan, F. (2005) Studies toward the pharmacophore of salvinorin A, a potent kappa opioid receptor agonist. *J. Med. Chem.* **48**, 345–348.

Nakano, C., Oshima, M., Kurashima, N. and Hoshino, T. (2015) Identification of a new diterpene biosynthetic gene cluster that produces O-methylkolavelool in *Herpetosiphon aurantiacus*. *ChemBioChem*, **16**, 772–781.

Nyiligira, E., Viljoen, A.M., Van Heerden, F.R., Van Zyl, R.L., Van Vuuren, S.F. and Steenkamp, P.A. (2008) Phytochemistry and in vitro pharmacological activities of South African *Vitex* (Verbenaceae) species. *J. Ethnopharmacol.* **119**, 680–685.

Omosa, L.K., Amugune, B., Ndunda, B., Milugo, T.K., Heydenreich, M., Yenesew, A. and Midiwo, J.O. (2014) Antimicrobial flavonoids and diterpenoids from *Dodonaea angustifolia*. *S. Afr. J. Bot.* **91**, 58–62.

Ono, M., Yamamoto, M., Masuoka, C., Ito, Y., Yamashita, M. and Nohara, T. (1999) Diterpenes from the fruits of *Vitex rotundifolia*. *J. Nat. Prod.* **62**, 1532–1537.

Ono, M., Sawamura, H., Ito, Y., Mizuki, K. and Nohara, T. (2000) Diterpenoids from the fruits of *Vitex trifolia*. *Phytochemistry*, **55**, 873–877.

Ono, M., Ito, Y. and Nohara, T. (2001) Four new halimane-type diterpenes, vitetrifolins D-G, from the fruit of *Vitex trifolia*. *Chem. Pharmaceut. Bull.* **49**, 1220–1222.

Ono, M., Yanaka, T., Yamamoto, M., Ito, Y. and Nohara, T. (2002) New diterpenes and norditerpenes from the fruits of *Vitex rotundifolia*. *J. Nat. Prod.* **65**, 537–541.

Ono, M., Yamasaki, T., Konoshita, M., Ikeda, T., Okawa, M., Kinjo, J., Yoshimitsu, H. and Nohara, T. (2008) Five new diterpenoids, viteagnusins A-E, from the fruits of *Vitex agnus-castus*. *Chem. Pharmaceut. Bull.* **56**, 1621–1624.

Ono, M., Nagasawa, Y., Ikeda, T., Tsuchihashi, R., Okawa, M., Kinjo, J., Yoshimitsu, H. and Nohara, T. (2009) Three new diterpenoids from the fruit of *Vitex agnus-castus*. *Chem. Pharmaceut. Bull.* **57**, 1132–1135.

Ono, M., Eguchi, K., Konoshita, M. *et al.* (2011) A new diterpenoid glucoside and two new diterpenoids from the fruit of *Vitex agnus-castus*. *Chem. Pharmaceut. Bull.* **59**, 392–396.

Paddon, C.J., Westfall, P.J., Pitera, D.J. *et al.* (2013) High-level semi-synthetic production of the potent antimalarial artemisinin. *Nature*, **496**, 528–532.

Pateraki, I., Andersen-Ranberg, J., Hamberger, B., Heskes, A.M., Martens, H.J., Zerbe, P., Bach, S.S., Moller, B.L., Bohlmann, J. and Hamberger, B. (2014) Manoyl oxide (13*R*), the biosynthetic precursor of forskolin, is synthesized in specialized root cork cells in *Coleus forskohlii*. *Plant Physiol.* **164**, 1222–1236.

Pateraki, I., Andersen-Ranberg, J., Jensen, N.B. *et al.* (2017) Total biosynthesis of the cyclic AMP booster forskolin from *Coleus forskohlii*. *eLife*, **6**, e23001.

Pelot, K.A., Mitchell, R., Kwon, M., Hagelthorn, D.M., Wardman, J.F., Chiang, A., Bohlmann, J., Ro, D.K. and Zerbe, P. (2017) Biosynthesis of the psychotropic plant diterpene salvinorin A: discovery and characterization of the *Salvia divinorum* clerodienyl diphosphate synthase. *Plant J.* **89**, 885–897.

Peters, R.J. (2010) Two rings in them all: the labdane-related diterpenoids. *Nat. Prod. Rep.* **27**, 1521–1530.

Pompon, D., Louerat, B., Bronine, A. and Urban, P. (1996) Yeast expression of animal and plant P450s in optimized redox environments. *Meth. Enzymol.* **272**, 51–64.

Riley, A.P., Groer, C.E., Young, D., Ewald, A.W., Kivell, B.M. and Prisinzano, T.E. (2014) Synthesis and kappa-opioid receptor activity of furan-substituted salvinorin A analogues. *J. Med. Chem.* **57**, 10464–10475.

Ro, D.-K., Ehlting, J. and Douglas, C.J. (2002) Cloning, functional expression, and subcellular localization of multiple NADPH-cytochrome P450 reductases from hybrid poplar. *Plant Physiol.* **130**, 1837–1851.

Scheler, U., Rothe, K., Manzano, D. *et al.* (2016) Engineering the biosynthesis of carnosic acid and carnosol in yeast. *Nat. Commun.* **7**, 12942.

Schellenberg, R. (2001) Treatment for the premenstrual syndrome with agnus castus fruit extract: prospective, randomised, placebo controlled study. *BMJ* **322**, 134–137.

Shul′ts, E.E., Mironov, M.E. and Kharitonov, Y.V. (2014) Furanoditerpenoids of the labdane series: occurrence in plants, total synthesis, several transformations, and biological activity. *Chem. Nat. Comp.* **50**, 5–22.

Smith, A.B., Toder, B.H., Carroll, P.J. and Donohue, J. (1982) Andrographolide: an X-ray crystallographic analysis. *J. Crystallograph. Spectroscop. Res.* **12**, 309–318.

Teoh, K.H., Polichuk, D.R., Reed, D.W. and Covello, P.S. (2009) Molecular cloning of an aldehyde dehydrogenase implicated in artemisinin biosynthesis in *Artemisia annua*. *Botany*, **87**, 635–642.

Tesso, H. and König, W.A. (2004) Terpenes from *Otostegia integrifolia*. *Phytochemistry*, **65**, 2057–2062.

Trikka, F.A., Nikolaidis, A., Ignea, C. *et al.* (2015) Combined metabolome and transcriptome profiling provides new insights into diterpene biosynthesis in *S. pomifera* glandular trichomes. *BMC Genom.*, **16**, 935.

Webster, D.E., He, Y., Chen, S.N., Pauli, G.F., Farnsworth, N.R. and Wang, Z.J. (2011) Opioidergic mechanisms underlying the actions of *Vitex agnus-castus* L. *Biochem. Pharmacol.* **81**, 170–177.

Wubshet, S.G., Tahtah, Y., Heskes, A.M., Kongstad, K.T., Pateraki, I., Hamberger, B., Møller, B.L. and Staerk, D. (2016) Identification of PTP1B and α-glucosidase inhibitory serrulatanes from *Eremophila* spp. by combined use of dual high-resolution PTP1B and α-glucosidase inhibition profiling and HPLC-HRMS-SPE-NMR. *J. Nat. Prod.* **79**, 1063–1072.

Wuttke, W., Jarry, H., Christoffel, V. and Spengler, B. (2003) Chaste tree (*Vitex agnus-castus*) – pharmacology and clinical indications. *Phytomedicine*, **10**, 348–357.

Xu, M., Hillwig, M.L., Prisic, S., Coates, R.M. and Peters, R.J. (2004) Functional identification of rice *syn*-copalyl diphosphate synthase and its role in initiating biosynthesis of diterpenoid phytoalexin/allelopathic natural products. *Plant J.* **39**, 309–318.

Yao, J.-L., Fang, S.-M., Liu, R., Oppong, M.B., Liu, E.-W., Fan, G.-W. and Zhang, H. (2016) A review on the terpenes from genus *Vitex*. *Molecules*, **21**, 1179.

Yee, N.K.N. and Coates, R.M. (1992) Total synthesis of (+)-9,10-*syn*- and (+)-9,10-*anti*-copalol via epoxy trienylsilane cyclization. *J. Org. Chem.* **57**, 4598–4608.

Zerbe, P., Hamberger, B., Yuen, M.M.S., Chiang, A., Sandhu, H.K., Madilao, L.L., Nguyen, A., Hamberger, B., Bach, S.S. and Bohlmann, J. (2013) Gene discovery of modular diterpene metabolism in nonmodel systems. *Plant Physiol.* **162**, 1073–1091.

Zerbe, P., Chiang, A., Dullat, H., O'Neil-Johnson, M., Starks, C., Hamberger, B. and Bohlmann, J. (2014) Diterpene synthases of the biosynthetic system of medicinally active diterpenoids in *Marrubium vulgare*. *Plant J.* **79**, 914–927.

Zheng, C.J., Huang, B.K., Wu, Y.B., Han, T., Zhang, Q.Y., Zhang, H. and Qin, L.P. (2010) Terpenoids from *Vitex negundo* seeds. *Biochem. Systemat. Ecol.* **38**, 247–249.

Zheng, C.J., Zhu, J.Y., Yu, W., Ma, X.Q., Rahman, K. and Qin, L.P. (2013) Labdane-type diterpenoids from the fruits of *Vitex trifolia*. *J. Nat. Prod.* **76**, 287–291.

Zi, J. and Peters, R.J. (2013) Characterization of CYP76AH4 clarifies phenolic diterpenoid biosynthesis in the Lamiaceae. *Org. Biomolec. Chem.* **11**, 7650–7652.